Water Science & Technology

IWA PUBLISHING



Water Science & Technology Vol 84 No 7, 1678 doi: 10.2166/wst.2021.378

# Production and modification of hydrochar from anaerobically digested cattail for adsorbing ammonium and phosphorous in wastewater

Sanjaya Ghimire, Lijun Wang*, Bo Zhang, Xin Li and Abolghasem Shahbazi

Department of Natural Resources and Environmental Design, North Carolina Agricultural and Technical State University, 1601 East Market Street, Greensboro, NC 27411, USA
*Corresponding author. E-mail: lwang@ncat.edu

BZ, 0000-0002-4599-7372

## ABSTRACT

Water contamination by nitrogen and phosphorus ions has a direct consequence of eutrophication to the ecosystem. The objective of this study is to investigate the production of hydrochars by acetic acid or sodium hydroxide assisted hydrothermal carbonization (HTC), various activation methods, and the potential of hydrochar as an adsorbent to remove $NH_4^+$-N and $PO_4^{3-}$-P from wastewater. The results showed that acetic acid or sodium hydroxide assisted HTC and activation with magnesium chloride or air could improve the surface properties of hydrochar. Acetic acid modification generated extensive oxygenated functional groups, while sodium hydroxide modification produced hydrochar with a high N/C ratio and surface aromaticity. Treating hydrochar with magnesium chloride could impregnate nano-magnesium particles on the hydrochar, thereby improving the ability to remove N and P. Air activation of hydrochar resulted in more oxygen containing functional groups. The $NH_4^+$-N and $PO_4^{3-}$-P adsorption capacities of these hydrochars ranged from 92.6 to 122.4 mg/g and 1.6 to 15.8 mg/g, respectively. The adsorption capacity of hydrochars in swine wastewater is similar to the results of artificial wastewater. The results suggested that Mg-nanoparticle dispersion and oxygen-containing functional groups played a major role in adsorption than ion exchange and physisorption.

**Key words:** adsorption, ammonium, hydrochar, isotherm, phosphorus

## HIGHLIGHTS

- Hydrochars were produced by acetic acid and sodium hydroxide assisted HTL.
- Magnesium chloride or air activation could improve the surface properties of hydrochar.
- Hydrochar activated by using $MgCl_2$ and air substantially increased the adsorption capacity.
- Mg-nanoparticle dispersion and oxygen containing functional groups played a major role in adsorption.

## GRAPHICAL ABSTRACT

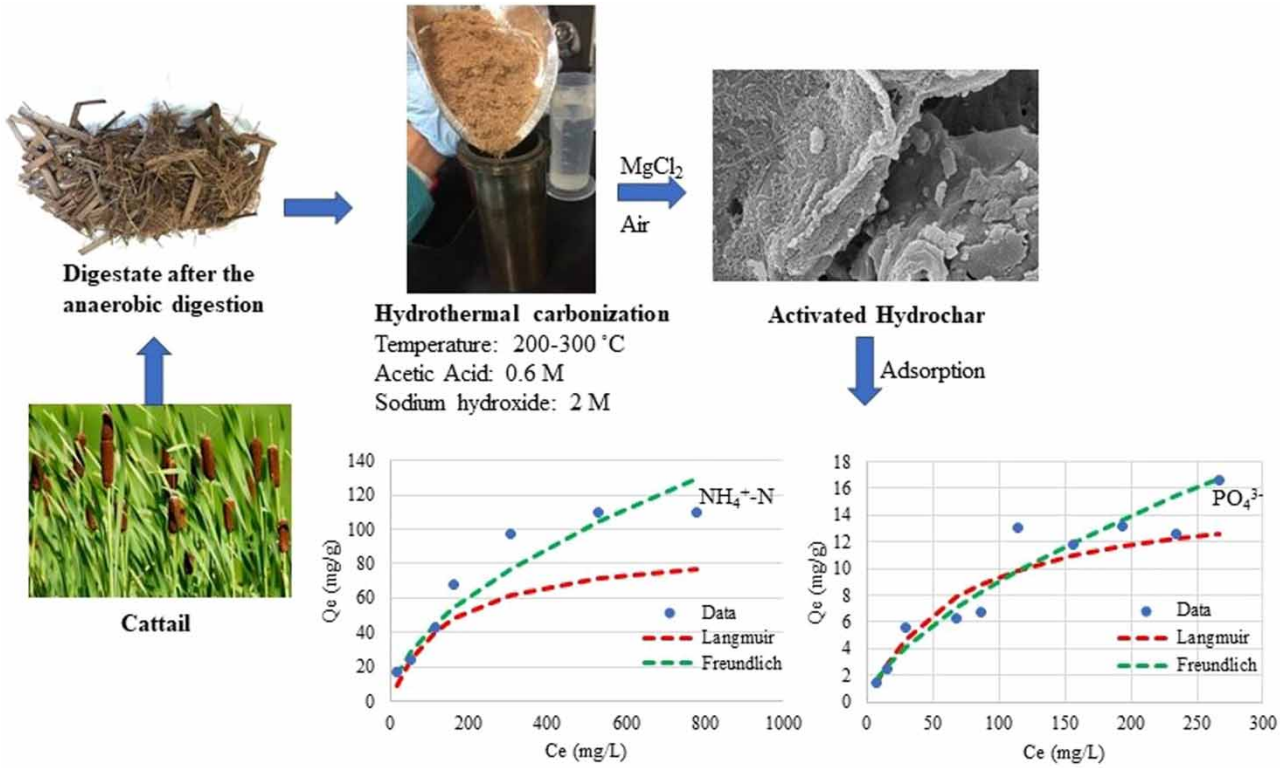


## INTRODUCTION

With the rapid development of modern society, a large number of human activities, such as excessive fertilization and dumping of industry and sewage, have caused nutrients to pollute water and affect rivers, lakes and ocean coasts (Goel 2006). This type of pollution causes direct environmental and human health problems, as well as impacts on the economy. Excessive nitrogen (N) and phosphorus (P) in wastewater discharge can lead to eutrophication of natural water, which results in the growth of algae in the water, lack of oxygen and the death of animal life (Khan & Mohammad 2014). Therefore, a wastewater treatment process is required to remove N and P from the effluent.

Nitrogen and phosphorus removal technologies are mainly divided into chemical, physical and biological methods. Chemical treatment may produce pollutants (such as sludge) due to the precipitation of phosphorus (Yamashita & Yamamoto-Ikemoto 2014). In terms of biological treatment, it is usually costly and slow because of the need for aeration, microbial growth and other pre-treatments (Bekoe *et al.* 2018). In the past few decades, physical methods such as reverse osmosis, electrodialysis and adsorption have attracted widespread attention. Due to low cost and high process efficiency, adsorption is widely used as a promising water purification method (Bolisetty *et al.* 2019). Research on effective and economical adsorbents to remove N and P in wastewater has considerable economic and environmental value (Takaya *et al.* 2016).

Biochar produced from agricultural wastes provides a viable adsorbent for removing phosphorus and nitrogen from wastewater. In addition, the nutrient-rich biochar after use can be developed into a high-value bio-fertilizer. However, the literature shows that the adsorption results of nitrogen and phosphorus on biochar from different sources and production processes are inconsistent. Kizito *et al.* (2015) showed that the biochar from wood could remove 73% of $NH_4^+$ from an ammonium solution, compared to 60% for the biochar from rice husk. The biochars prepared from wood and rice husk could remove 60 and 53% of $NH_4^+$ in the anaerobic digestate (Maurer *et al.* 2017). Takaya *et al.* (2016) suggested that the surface area might not be the most important factor that affected the physisorption of ammonia. Jung *et al.* (2015) showed that the surface area of biochar increased with increasing treatment temperature from 200 to 400 °C, and its P adsorption capacity increased accordingly.

Although the specific adsorption mechanism is still unclear, the presence of functional groups and metals may play a key role in the adsorption of N and P (Takaya *et al.* 2016).

In the past few years, hydrothermal carbonization (HTC) has gained a considerable attention for producing hydrochar (a typical biochar) from carbonaceous materials with a high moisture content (such as municipal sludge, manure, algae, and kitchen waste) (Zhang *et al.* 2020). HTC processes the feedstock under a self-generated pressure at a mild temperature (e.g., 250 °C) to produce solid hydrochar and aqueous solution containing organic and inorganic compounds. Also, HTC can destroy pathogens, eliminate odors, and remove heavy metals from raw materials. The product of hydrochar is a more hydrophobic solid than that produced by dry torrefaction, which in turn has positive correlation with carboxylic groups on the biochar surface, specific surface area, and pore volume (Xiu *et al.* 2017; Mao *et al.* 2019). It has been reported that various factors such as the cation exchange capacity, oxygen containing/acidic functional groups, available anion exchange sites and surface charges, and initial concentration of pollutants affect the adsorption of N and P over hydrochar (Kameyama *et al.* 2012; Chintala *et al.* 2014).

In this study, cattail (*Typha* species) is used as the feedstock, which is a kind of aquatic plant commonly grown on wetlands. It has high insect resistance, high adaptability and high reproduction ability (Zhang *et al.* 2012). The annual productivity of cattails is considerably high. It was reported that standing crop yields up to 22.4 Mg $ha^{-1}$ of leaves and 30.9 Mg $ha^{-1}$ of rhizomes (Dubbe *et al.* 1988). Improper management of cattails may cause corruption in water, severe secondary pollution, rapid marshes of lakes, and reduced invertebrate production and migratory birds (Kostecke 2002). Studies have shown that harvesting half of the cattails grown in wetlands every year (including rhizomes) will not affect its growth and progress next year (Bansal *et al.* 2019). Because of these advantages, cattails are considered as a potential renewable feedstock for bioenergy production. Glacial acetic acid ($CH_3COOH$) or sodium hydroxide (NaOH) were used to assist the HTC process of cattails. Both acetic acid and sodium hydroxide have been shown to accelerate the degradation/hydrolysis of the dairy manure and improve the biochar's quality (Chen *et al.* 2018). The obtained hydrochar was further activated by using $MgCl_2$ or air. To the best of our knowledge, this is the first study on the influence of chemical-assisted HTC of the anaerobic digestate and subsequent $MgCl_2$ or air activation on the N and P adsorption capacity of hydrochar. The objective of this study is to (1) compare the N and P adsorption capacity of hydrochar produced under different HTC temperatures, chemical modification and $MgCl_2$ or air activation; (2) study the N and P adsorption capacity of various hydrochars prepared from anaerobic digested cattail in artificial wastewater and swine wastewater. The research results provide a theoretical and practical basis for the development of hydrochar adsorbents for N and P adsorption from wastewater.

## MATERIALS AND METHODS

### Materials

Cattail (*Typha latifolia*), the anaerobic digestion (AD) process, and the composition of cattail digestate have been described elsewhere (Zhang *et al.* 2020). Cattail was anaerobically digested for 14 days, collected after AD, washed with deionized water to remove loose contents, dried at 105 °C for 24 h in a Thermo Scientific Precision Compact Oven (Waltham, MA, USA). About 2 kg (dry basis) of anaerobically digested cattails were prepared and stored at room temperature for future use.

Artificial wastewater was prepared according to the procedure reported in the literature (Fang *et al.* 2014). For P-containing wastewater, potassium phosphate monobasic was used for the preparation of the phosphate solution at 125 mg/L. Ammonium hydroxide was used to prepare the N-containing wastewater at a concentration of at 1,000 mg/L. These two solutions were diluted to various concentrations for the measurement of adsorption isotherms.

Swine wastewater was collected from the uncovered lagoon at the swine research facility of the University, which represents a low-strength wastewater. Pretreatment of swine wastewater was carried out by sedimentation and filtration with a Whatman quantitative filter paper with 8 μm pore size to remove large, non-soluble particulate solids.

### Hydrothermal carbonization

Approximately 10 g of dried feedstock was mixed with 160 mL of deionized water into a 300 ml stirred Parr reactor (Parr Instrument, Moline, IL, USA). For chemical-assisted HTC, glacial acetic acid ($CH_3COOH$) or sodium hydroxide (NaOH) was added with 160 mL water, giving a concentration of 0.6 M and 2 M, respectively. The choice of the concentrations is based on the results reported in the literature (Reza *et al.* 2015; Wang *et al.* 2017).

The temperature of the reactor was increased at a heating rate of about 10 °C/min and held at the desired temperature for 1 h. HTC was performed at three different temperatures of 200, 250 and 300 °C and the stirring speed was set at 100 rpm. The

hydrochar produced via water-only, acetic acid-assisted, and sodium hydroxide-assisted HTC at various temperatures was denoted as B200/B250/B300, AB200/AB250/AB300, and NB200/NB250/NB300, respectively.

After HTC treatment, the reactor was cooled down to the room temperature. The hydrochar was filtered out using Whatman grade 1 filter paper and washed with deionized water and ethanol to remove residual bio-oil. The hydrochar was then dried in an oven at 105 °C for 24 h and ground into powder for further analysis. The yield of hydrochar was calculated as:

$$Hydrochar\ yield = \frac{Mass\ of\ hydrochar}{Mass\ of\ raw\ biomass} * 100\% \quad (1)$$

## Activation of hydrochar

Molten salt activation of hydrochar was prepared with $MgCl_2$, which is one of the common molten salts for activation. For a typical process, the hydrochar (B250) was mixed with $MgCl_2$ at a mass ratio of 1:1, and then the mixture was homogenized with a mortar and pestle. The powdered mixture was transferred to a ceramic crucible and was placed in an electric furnace equipped with a continuous nitrogen flow. After flushing with nitrogen for 30 min, the furnace was ramped at 10 °C/min to the carbonization temperature of 600, 700 or 800 °C and kept at this temperature for 1 h. The furnace was cooled to ambient temperature by switching off the power; meanwhile, the nitrogen flow was maintained until the temperature reached room temperature. The as-obtained product was washed with sufficient amount of water to remove the salts. The activated hydrochar was dried in an oven at 105 °C for 12 h. Hydrochars carbonized at 600, 700 and 800 °C were denoted as MB600, MB700, and MB800, respectively. The yields of hydrochars defined by Equation (1) are reported in the Results and Discussion section.

Air activation of the hydrochar (B250) was conducted at 250 °C. For a typical run, 5 g of hydrochar was heated from the room temperature to activation temperature of 250 °C in an air stream. The sample was held at 250 °C for 2 hr. Then, under the same flow of air, the system was allowed to cool down to the room temperature. The hydrochar was designated as air activated hydrochar.

## Characterization

Physical nitrogen adsorption, pore volume, and pore size were measured using a Micromeritics ASAP 2020 surface area and porosity analyzer (Norcross, GA, USA).

Thermogravimetric analyses (TGA) were performed using a TA Instruments SDT Q600 thermogravimetric analyzer (New Castle, DE, USA), in which samples were heated to 250 °C at a heating rate of 20 °C/min in nitrogen.

The morphology of hydrochars was evaluated using a JEOL 7500F scanning electron microscope (SEM, Tokyo, Japan). Energy-dispersive X-ray spectroscopy (EDX) analysis of hydrochar was performed on a JEOL 7500F SEM coupled with an energy dispersive X-ray detector. For each sample (total 13 different hydrochars), the measurement was carried out on 5–10 different particles.

The absorption spectroscopy in the infrared region was measured to determine the frequency of vibrations of the functional groups present in the hydrochar. The spectrum readings were obtained using an Agilent 670 Fourier transform infrared (FTIR) spectrometer with attenuated total reflection (ATR) varied in the range of 4,000–400 $cm^{-1}$ (Santa Clara, CA, USA).

## Ammonium and phosphate adsorption

To evaluate the adsorption capacity of hydrochar to ammonium, 0.1 g of hydrochar was mixed with 100 mL ammonium hydroxide solution in a beaker. The mixture was then shaken on a shaker at 160 rpm and 25 °C for 24 h. After that, the mixture was filtered through a 0.45 μm membrane, and then the ammonium concentration was determined using the TNT 830 ammonia kit with a Hach 6000 UV/VIS spectrophotometer (Loveland, CO, USA).

The same procedure was used to measure the adsorption capacity of hydrochar to phosphate using 125 mg/L phosphate solution. Phosphate concentration of the filtrate was determined using the TNT 845 kit with the Hach spectrophotometer. The adsorption experiments were performed in triplicate, and the average values were reported.

The adsorption capacity Q (mg $g^{-1}$) of the hydrochar was calculated as:

$$Q = (Co - Ce)\frac{V}{m} \quad (2)$$

where $C_e$ and $C_0$ are the equilibrium and initial $NH_4^+$-N or $PO_4^{3-}$-P concentrations (mg/L), respectively. V is the volume of the solution and m is the weight of hydrochar (g).

For the adsorption test in swine wastewater, 0.1 g of hydrochar was mixed with 100 mL diluted swine wastewater in a beaker. The mixture was then shaken on a shaker at 160 rpm and 25 °C for 24 h. After that, the mixture was filtered through a 0.45-μm membrane and analyzed for the chemical oxygen demand (COD), $NH_4^+$-N, and total phosphorus (TP).

### Adsorption isotherms and mathematical models

To measure the adsorption isotherm of ammonium, 0.1 g of the hydrochar was mixed with 50 mL ammonium hydroxide solution with different initial concentrations of 25, 50, 100, 200, 300, 500, 750, and 1,000 mg/L. All samples were shaken on the mechanical shaker at 160 rpm and 25 °C for 24 h. The samples were filtered through a 0.45-μm membrane, and then the ammonium concentration was determined immediately with the Hach spectrophotometer. Based on the difference between the initial and final solution concentrations, ammonium adsorbed on the hydrochar was calculated. To measure the adsorption isotherm of phosphorus, 0.1 g of the hydrochar was mixed with 50 mL phosphate solution with initial concentrations of 20, 50, 80, 100, 150, 200, 250, 300, and 350 mg/L. The remaining procedure was the same as that of ammonium. All isotherm experiments were performed in triplicate, and the average values reported.

The Langmuir and Freundlich models were used for the regression of the adsorption isotherm. The equations of these two models are written as:

$$\text{Langmuir: } Q_e = \frac{K_L S_{max} C_e}{1 + K_L C_e} \tag{3}$$

$$\text{Freundlich: } Qe = K_F C_e^{1/n} \tag{4}$$

where $K_L$ and $K_f$ are the Langmuir bonding term related to interaction energies (L/mg) and the Freundlich affinity coefficient ($mg^{(1-n)}L^n/g$), respectively. $S_{max}$ is the Langmuir maximum capacity (mg/kg), $Ce$ is the equilibrium solution concentration (mg/L) of the sorbate, and $n$ is the Freundlich linearity constant.

## RESULTS AND DISCUSSION

### Hydrochar production and activation

HTC of anaerobically digested cattails was conducted in deionized water, acetic acid solution and sodium hydroxide solution at 200, 250 and 300 °C for 1 h. The hydrochar yields are summarized in Figure 1. The reaction temperature showed an obvious effect on the hydrochar yield. When the temperature increased from 200 to 300 °C, the hydrochar yields decreased

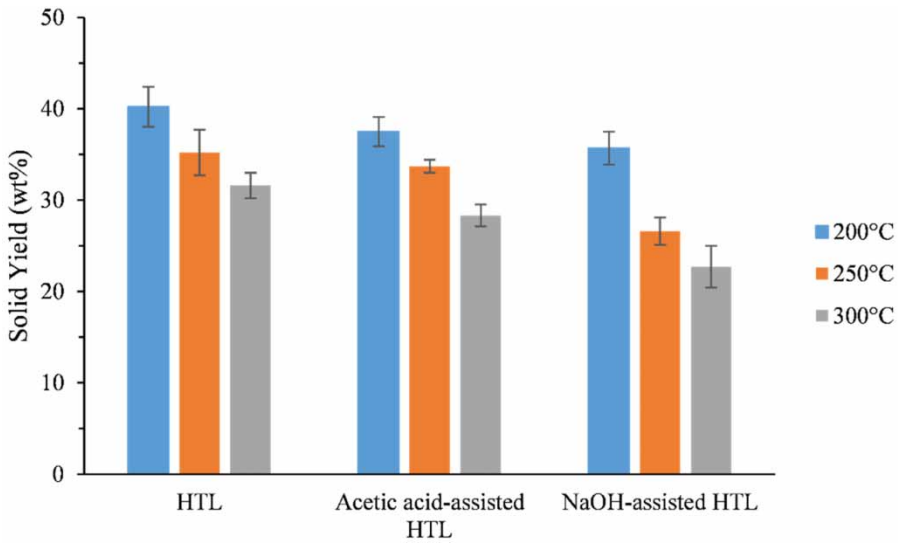


**Figure 1** | Solid yields of hydrochar under different conditions.

from 40.2% to 31.6%, 37.5% to 28.3%, and 35.7% to 22.7% for the use of water, acetic acid, and sodium hydroxide, respectively.

On average, the increase of the temperature from 200 °C to 300 °C reduced the solid yield by 7–9% of the original mass. The loss of biomass during HTC at a low temperature was mainly attributed to the decomposition of the hemicellulose component. As a result, the hydrochar product treated at 200 °C still showed a color similar to the original feedstock. When the temperature increased, cellulose degradation starts to occur at a temperature above 200 °C due to disintegration through hydrolytic action and further reactions, decreasing the hydrochar yield (Volpe *et al.* 2018). Because of the *p*-value of one-way ANOVA analysis (Table S1), the application of acetic acid and sodium hydroxide significantly decreased the hydrochar yield at 250–300 °C (i.e., $p$-value $< 0.05$) compared with water-only HTC, which may be caused by the higher hydrolytic effect caused by chemicals added. It is well known that acetic acid could enhance the degradation of hemicellulose and cellulose, while sodium hydroxide could dissolve lignin and partial hemicellulose (Zhang & Wang 2013).

Because raw hydrochars and acetic acid/sodium hydroxide modified hydrochars showed similar properties and adsorption capacity, B250 hydrochar was chosen for further activation. $MgCl_2$ activation of B250 hydrochar was conducted at 600, 700 and 800 °C, and the yield of activated hydrochar was approximately 90% of the original hydrochar. Air activation process was simulated by using TGA. Figure 2 shows the TGA-DSC profiles of B250 hydrochar activated in air. When the temperature increased from the ambient temperature to 250 °C, the weight loss can be divided into two phases (Figure 2(a)). The first phase was between the ambient temperature and 150 °C, which was due to the loss of water present in various forms and represented about 3.5 wt% of the total hydrochar weight. At this stage, the process was endothermic. The second phase happened between 200 and 250 °C, representing a weight loss of approximately 0.5 wt%. The weight loss in the second phase might be due to volatilization of organic matters or oxidation. If the hydrochar was held at 250 °C for 2 h, it would cause an additional 20% mass loss. The process became exothermic (Figure 2(b)).

## Characterization of hydrochar

### Surface area

Table 1 gives the surface area of HTC hydrochars and activated hydrochars. The BET surface area of HTC hydrochars increased with the HTC temperature. The HTC hydrochar produced with deionized water at 200, 250 and 300 °C had a relatively small surface area of 4.40, 4.95 and 8.96 $m^2/g$, respectively. These values matched the results reported in the literature (Jaruwat *et al.* 2018). Hydrochars produced via acetic acid and sodium hydroxide-assisted HTC showed a similar trend. According to the *p*-value of one-way ANOVA analysis (Table S2), the surface area of hydrochars obtained at 300 °C was significantly higher than that of hydrochars obtained at 200–250 °C. When the temperature increased from 200 to 300 °C, the BET surface areas of the hydrochars increased from 2.52 to 6.86 $m^2/g$ and 4.71 to 7.42 $m^2/g$ for acetic acid and sodium hydroxide treated samples, respectively. This trend might be caused by the gradual degradation of organic matter in the feedstock and the formation of new vascular bundle and channel structure during the HTC process. But the difference of the surface area of hydrochars obtained via water-only hydrothermal liquefaction (HTL), acid-assisted HTL and base-assisted HTL was not significant.

Compared with HTC hydrochars, hydrochars activated with $MgCl_2$ showed higher BET surface areas, which were $84.85 \pm 1.22$, $131.53 \pm 2.47$, $151.02 \pm 2.86$ $m^2/g$ for 600, 700, and 800 °C treated samples, respectively. Nano-sized MgO dispersion on the hydrochar surface may increase the specific surface area of Mg-loaded hydrochars, which is further illustrated by the SEM images and the magnesium content obtained by the elemental analysis. The hydrochar activated in air at 250 °C showed the highest BET surface area (337.75 $m^2/g$) among all modified hydrochars. Activation in the presence of air leads to the development of porosity, mostly due to the generation of micropores and mesopores (Sajjadi *et al.* 2019).

### Scanning electron microscopy and EDX analysis

SEM images of hydrochars are shown in the supplementary material (Figure S1). SEM analysis of hydrochars allows the visualization of the surface characteristics of the materials. In hydrochars produced via HTC at 200–300 °C, the appearance of a rough surface and a rupture into scales were observed, which may be due to the intrinsic nature of the hydrochar matrix. Chemical modification with acetic acid and sodium hydroxide resulted in considerable cracks and fine particles attached to the surface, forming a system of micro-pore networks. In addition, the sodium hydroxide-modified hydrochar showed sodium hydroxide crystals on the surface, and the length of the crystals was between 1–2 μm.

The morphology of magnesium chloride-treated hydrochars is largely dependent on the treatment temperature. When treating at 600 and 700 °C, a large number of $MgCl_2$ crystal structures emerged and covered the surface. When a treatment

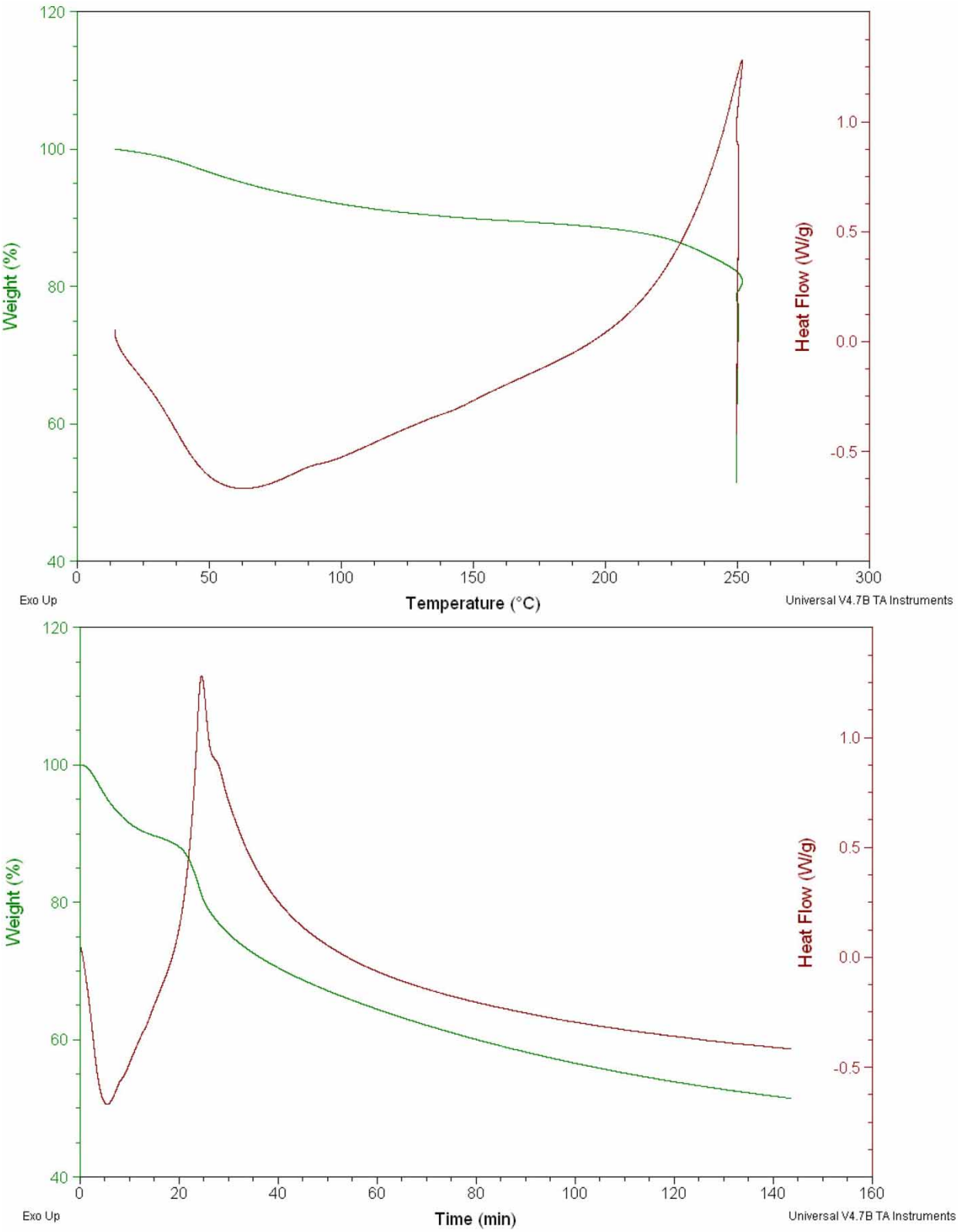


**Figure 2** | TGA-DSC graphs of B250 hydrochar, which was heated from 20 °C to 250 °C at 20 °C/min and held at 250 °C for 2 h. (a) Weight/heat flow vs. temperature, (b) weight/heat flow vs. time.

**Table 1** | Surface area of different hydrochar samples

| Sample ID | Specific surface area ($m^2/g$)[a] | t-plot micropore area ($m^2/g$) | Pore volume ($cm^3/g$) |
|---|---|---|---|
| B200 | 4.40 | – | 0.0091 |
| B250 | 4.95 | – | 0.017 |
| B300 | 8.96 | 1.11 | 0.0139 |
| AB200 | 2.52 | – | 0.0087 |
| AB250 | 2.85 | 0.69 | 0.0099 |
| AB300 | 6.86 | 1.85 | 0.0137 |
| NB200 | 4.71 | – | 0.0101 |
| NB250 | 5.62 | – | 0.01 |
| NB300 | 7.42 | 1.29 | 0.0161 |
| MB600 | 84.85 | 46.68 | 0.125 |
| MB700 | 131.53 | 94.80 | 0.125 |
| MB800 | 151.02 | 108.57 | 0.161 |
| Air activated hydrochar | 337.75 | 286.96 | 0.249 |

[a]The average values of three samples were reported, and the standard deviation was between 0.3 and 3.

temperature of 800 °C was used, molten salt activation happened, and the molten $MgCl_2$ corroded the carbonaceous material to form more cracks and voids, resulting in a higher surface area. These finding are backed up by similar results reported by Fang *et al.* (2014) in magnesium-modified corn hydrochar. Air-activated hydrochar showed more cracks and carbon particles on the surface compared with B250 hydrochar.

Table 2 gives the elemental compositions of the raw and modified hydrochars determined by EDX. The dominant elements were carbon and oxygen, which were from 59.98% to 82.49% and 11.35% to 32.28%, respectively. Generally, the hydrochar obtained at 200 °C had the lowest carbon content, indicating incomplete volatilization. Hydrochars produced at 250 and 300 °C showed a similar quality. Because a 250 °C HTC could give a higher hydrochar yield, 250 °C was considered as the optimal HTC temperature in this study. Therefore, hydrochar obtained via the 250 °C HTC was further used for activation.

The hydrochars also had trace amounts of phosphorus, magnesium, potassium, calcium, and sulfur. Sodium hydroxide-assisted HTC yielded hydrochar with a higher amount of sodium, which is the residue of sodium hydroxide. The presence of magnesium contents on magnesium modified hydrochar is related to the amount of $MgCl_2$ used and the carbonization temperature. The loading of magnesium was between 3.64 and 4.02%. Carbonization at 800 °C considerably reduced the chlorine content of the material, while at 600 °C or 700 °C, magnesium still existed in the form of $MgCl_2$. These results were further corroborated by the dispersion of Mg on the surface and enhanced surface area. The oxygen content of air activated hydrochar increased at the expense of the carbon content, which is attributed to the oxidation of the material.

**Table 2** | Elemental composition results of hydrochars

| | B200 | B250 | B300 | AB200 | AB250 | AB300 | NB200 | NB250 | NB300 | MB600 | MB700 | MB800 | Air activated |
|---|---|---|---|---|---|---|---|---|---|---|---|---|---|
| C | 66.37 | 73.64 | 73.59 | 73.68 | 74.92 | 75.66 | 59.98 | 63.48 | 63.19 | 77.46 | 82.34 | 82.49 | 67.61 |
| O | 31.62 | 25.32 | 25.11 | 24.70 | 24.76 | 24.27 | 31.24 | 27.67 | 27.03 | 18.25 | 13.36 | 11.35 | 32.28 |
| P | 0.93 | 0.44 | 0.31 | 0.47 | 0.12 | – | 0.47 | 1.06 | 0.72 | 0.83 | 0.66 | 0.62 | – |
| S | 0.16 | 0.07 | 0.16 | 0.22 | 0.12 | 0.12 | 0.097 | 0.12 | 0.15 | – | – | – | 0.04 |
| Ca | 1.41 | 0.95 | 0.66 | 0.82 | 0.48 | – | 1.31 | 3.25 | 2.08 | 1.37 | 1.27 | 1.32 | – |
| Na | – | – | – | – | – | | 6.66 | 3.82 | 6.36 | – | – | – | – |
| K | 0.19 | 0.29 | – | – | – | – | – | | | – | – | – | 0.07 |
| Mg | 0.15 | 0.22 | 0.19 | 0.11 | 0.15 | | 0.11 | 0.21 | 0.39 | 3.64 | 3.65 | 4.02 | – |
| Cl | – | – | – | – | – | – | – | – | – | 2.95 | 3.51 | 0.16 | – |

### FTIR analysis

The analysis of functional groups on the surface of hydrochars could help to determine the mechanisms responsible for the adsorption of nutrients in the structure of these materials. The infrared spectra of hydrochars are shown in Figure 3.

The FTIR analysis demonstrated that the character peaks of modified hydrochars differed from each other. The peak at approximately 3,445 $cm^{-1}$ corresponded to the O–H stretching vibration, which changed noticeably for $MgCl_2$ and acetic acid modified samples. The weakened peak of the O–H vibration indicates the structural change of the feedstock under these chemical treatments. Peaks obtained between 2,820 and 2,990 $cm^{-1}$ suggested the stretching vibrations of aliphatic C-H. This peak indicated the presence of aliphatic structure in hydrochar samples. The band at 1,737 $cm^{-1}$ indicated the C = O stretching vibrations in all modified hydrochar, suggesting hemicellulose degradation during HTC above 200 °C. The peak at 1,698 $cm^{-1}$ corresponding to the carboxyl, ester or carbonyl groups was seen in all hydrochars with little difference, indicating the presence of oxygen-containing functional groups on the hydrochar surface. However, this peak was not clearly noticeable in magnesium-modified hydrochar at 800 °C, which may be due to increased oxygen loss caused by thermal degradation and decarboxylation (Reza *et al.* 2015). This loss of oxygen in magnesium-modified hydrochar at higher temperature is supported by elemental analysis as well. The adsorption peak at 1,508 and 1,460 $cm^{-1}$ indicated the presence of aromatic lignin groups in the sample. However, the flattened peak at higher temperature magnesium-modified hydrochar suggested the partial degradation of lignin.

Overall, magnesium modification did not affect the structural formation of most organic functional groups in Mg/hydrochar. The character peaks at 3,200 $cm^{-1}$ –3,700 $cm^{-1}$, 1,400 $cm^{-1}$ –1,690 $cm^{-1}$, and 550 $cm^{-1}$ –850 $cm^{-1}$ represented the hydroxyl (O–H), double bonds (C = O and C = C), and organic chloride (C–Cl), respectively. Air activation reduced certain structures of the hydrochar. But air activated hydrochar was still rich in functional groups of O–H, C = C, carbonyl group, C-O, and so on.

### $NH_4^+$-N and $PO_4^{3-}$-P adsorption

Factors including initial $NH_4^+$ concentration, pH, and contact time with solution could determine the adsorption capacity of hydrochar. In this study, the pH of the solution was adjusted to neutral as it has been shown to favor $NH_4^+$-N adsorption (Banerjee *et al.* 2014). As shown in Table 3, hydrochar produced by HTC resulted in around 10% of $NH_4^+$-N removal from the artificial wastewater. Hydrochar produced by water-only and acetic acid-assisted HTC resulted in a $PO_4^{3-}$-P removal of 2–3%. Sodium hydroxide modification of the hydrochar at 250 and 300 °C increased the $PO_4^{3-}$-P adsorption to ~4.5%. Increased surface area and addition of functional groups may contribute to the increased adsorption capacity.

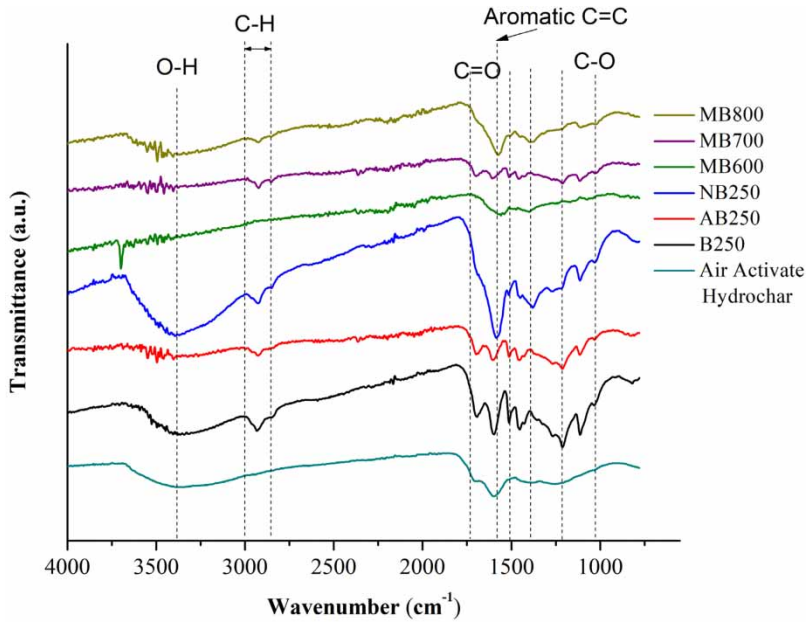


**Figure 3** | Infrared spectra of hydrochars.

**Table 3** | Adsorption capacity of hydrochars

| | Qe (mg $g^{-1}$) | % $NH_4^+$-N adsorbed | Qe (mg $g^{-1}$) | %$PO_4^{3-}$-P adsorbed |
|---|---|---|---|---|
| Raw hydrochars | | | | |
| B200 | 108.7 ± 3.2 | 10.87 | 3.1 ± 0.2 | 2.5 |
| B250 | 100.7 ± 0.7 | 10.07 | 3.3 ± 0.7 | 2.8 |
| B300 | 97.3 ± 1.6 | 9.73 | 2.6 ± 0.36 | 2.1 |
| Acetic acid hydrochars | | | | |
| AB200 | 112.4 ± 2.6 | 11.2 | 3.2 ± 0.9 | 2.5 |
| AB250 | 106.2 ± 2.9 | 10.6 | 3.7 ± 1.2 | 2.9 |
| Sodium hydroxide hydrochars | | | | |
| NB200 | 95. 5 ± 2.5 | 9.5 | 1.6 ± 2.6 | 1.3 |
| NB250 | 92.6 ± 3.2 | 9.2 | 5.6 ± 3.8 | 4.5 |
| NB300 | 87.4 ± 1.8 | 8.7 | 5.7 ± 8.4 | 4.6 |
| Magnesium-modified hydrochars | | | | |
| MB600 | 122.4 ± 2.2 | 12.2 | 11.7 ± 0.7 | 9.4 |
| MB700 | 118.6 ± 2.7 | 11.8 | 10.5 ± 1.3 | 8.4 |
| MB800 | 115.8 ± 6.1 | 11.5 | 11.9 ± 3.9 | 9.6 |
| Air-activated hydrochar | 112.4 ± 3.4 | 11.2 | 15.8 ± 2.3 | 12.6 |

Magnesium chloride modification of the hydrochar (B250) increased the adsorption capacity of both $NH_4^+$-N and $PO_4^{3-}$-P to ~12% and ~9.5%, respectively. Compared with the B250 hydrochar, the adsorption capacity of $MgCl_2$-activated hydrochar increased by 20 and 240%, respectively. The $NH_4^+$-N adsorption capacity of hydrochar prepared from AD digestate is similar or higher than the results reported in the literature, while the $PO_4^{3-}$-P adsorption capacity is lower than the results reported in the literature. Takaya *et al.* (2016) reported that $NH_4^+$-N and $PO_4^{3-}$-P adsorption capacities of hydrochar ranged from about 105.8–146.4 mg $g^{-1}$ and 0 to 30 mg $g^{-1}$, respectively. Another study showed that the cassava straw and banana straw biochars exhibited the theoretical maximum saturated adsorption capacities of 24.04 mg·$g^{-1}$ ($NH_4^+$-N) and 31.15 mg·$g^{-1}$ (TP), respectively (Jiang *et al.* 2019). They suggested that the magnesium loading had strong correlation with $NH_4^+$-N and $PO_4^{3-}$-P adsorption. In this study, surface area and pore volume showed moderate and weak correlation for $NH_4^+$-N and $PO_4^{3-}$-P adsorption, respectively. The improved $NH_4^+$-N adsorption capacity may be due to the presence of increased negatively-charged functional groups like carboxyl group. Increased $PO_4^{3-}$-P adsorption capacity could be attributed to surface complexation with hydroxyl functional group and Mg-phosphate precipitation reaction (Jiang *et al.* 2019).

Air-activated hydrochar had the most influential impact on P adsorption as it resulted in 15.8 mg/g of P adsorption and 12.6% removal from wastewater. Meanwhile, it also showed a slightly higher $NH_4^+$-N adsorption capacity. High surface area of air activated hydrochar (337.75 $m^2$/g) may have allowed high adsorption of both $NH_4^+$-N and $PO_4^{3-}$-P. Additionally, the increase in negative surface charge due to the presence of acidic functional groups such as the carbonyl group in air-activated hydrochar may have favored the N sorption capacity.

### Adsorption capacity in swine wastewater

Swine wastewater was used to test the adsorption capacity of hydrochars, which contained 1,470 mg/L COD, 50 mg/L $NH_4^+$-N and 151 mg/L TP. The phosphorus adsorption capacity of hydrochars in swine wastewater is similar to the results of artificial wastewater, which is within a range of 1.5–5.8 mg/g (Table 4). Because the swine wastewater collected from the open lagoon contained a small amount of $NH_4^+$-N, almost 100% of $NH_4^+$-N was removed by hydrochars. However, with the exception of air-activated hydrochar, most hydrochars had leaching problems. Therefore, before using hydrochar or activated carbon as an adsorbent to treat wastewater, pretreatment is required to reduce leaching.

### Ammonia and phosphate adsorption isotherms

Based on the initial evaluation, the following five hydrochars were selected for the adsorption isotherm study, including B250, AB250, NB250, MB800, and air-activated hydrochar. The results were fitted into Equations (2) and (3).

**Table 4** | Adsorption capacity of hydrochars in swine watstewater

| | COD (mg $g^{-1}$) | $NH_4^+$-N adsorbed (mg $g^{-1}$) | TP (mg $g^{-1}$) |
|---|---|---|---|
| Raw hydrochars | | | |
| B250 | N/A | 23.7 ± 0.7 | 1.8 ± 0.5 |
| AB250 | N/A | 24.5 ± 0.5 | 2.1 ± 0.3 |
| NB250 | N/A | 24.6 ± 1.2 | 2.5 ± 0.7 |
| Magnesium-modified hydrochars | | | |
| MB600 | N/A | 24.2 ± 0.4 | 2.3 ± 0.9 |
| MB700 | N/A | 24.8 ± 0.2 | 2.4 ± 1.1 |
| MB800 | N/A | 24.7 ± 0.6 | 2.2 ± 1.9 |
| Air-activated hydrochar | 135.1 ± 5.5 | 25.0 ± 0.4 | 5.8 ± 1.2 |

Figures 4 and 5 show the adsorption capacities of hydrochars on $NH_4^+$-N and $PO_4^{3-}$-P, respectively. For $NH_4^+$-N adsorption, the increase in initial concentration up to 300 mg/L showed a sharp increase in the adsorption capacity by hydrochars and stabilized at higher initial concentration. The $PO_4^{3-}$ adsorption showed a similar pattern, in which there was a rapid increase of adsorption capacity with the increase of initial concentration up to 150 mg/L and stabilization at higher initial concentration. Adsorption equilibrium concentration was reached after 24 h at room temperature for both $NH_4^+$-N and $PO_4^{3-}$-P. Adsorption equilibrium may have resulted in such phenomena. Compared with $PO_4^{3-}$-P, overall higher adsorption of $NH_4^+$-N might be due to the intrinsic negative charge of hydrochar that is not conducive for P adsorption.

The isotherm parameters for both models with the linear regression coefficient ($R^2$) are presented in Table 5. The $R^2$ value suggested that the Freundlich model fits the $NH_4^+$-N adsorption data better than the Langmuir model for most types of hydrochar. Typically, the Freundlich model indicates heterogenous and multilayer adsorption. Therefore, the results suggest that adsorption could be described by heterogenous and multilayer adsorption. This in turn implies that N adsorption by hydrochar is a sum of all the adsorption sites, where stronger binding sites are occupied first. The maximum adsorption capacity of $NH_4^+$-N by B250, AB250, NB250, MB800, and air-activated hydrochar were 147.08, 100, 98.04, 98.04, and 90.90 mg/g, respectively. The results showed that although the adsorption capacity increased at the initial $NH_4^+$-N concentration, the saturation of adsorption sites during the isotherm adsorption process led to a decrease in the adsorption capacity at a higher initial concentration. The maximum $NH_4^+$-N adsorption capacity of hydrochars has the following order: B250 > AB250 > NB250 = MB800> air-activated hydrochar.

From Table 5, the $R^2$ value indicates that the results of $PO_4^{3-}$-P adsorption also fit the Freundlich model better than the Langmuir model. The Freundlich model suggests that the adsorption of P is heterogeneous and multilayer, which is due to the diversity of adsorption sites and the nature of ions as free or hydrolyzed substances. The literature also showed that the Freundlich model suits phosphate adsorption better because of saturated adsorbents or precipitation reactions (Zeng *et al.* 2013). The maximum $PO_4^{3-}$-P adsorption capacity of hydrochars has the following order: air-activated hydrochar > MB800 > AB250 > NB250 > B250.

The adsorption intensity or surface heterogeneity (1/n) for all hydrochars on both N and P adsorption was less than 1. This value below unity indicates that the adsorption process is primarily governed by the chemisorption process (Oginni *et al.* 2020). Although not fully understood, it is suggested that the surface area has little effect on adsorption compared to its elemental composition. Xue *et al.* (2009) reported that chemical composition of adsorbent led to simultaneous ligand exchange and chemical precipitation between adsorbent and $PO_4^{3-}$-P. Previous studies have also suggested that surface functionality may not greatly influence phosphate adsorption since biochars tend to be negatively charged (Zeng *et al.* 2013).

## CONCLUSION

This study investigated anaerobically digested cattail hydrochars obtained via acetic acid or sodium hydroxide assisted HTC, various activation methods, and the N and P adsorption capacities of these hydrochars. When the HTC temperature increased from 200 to 300 °C, the hydrochar yields decreased from 40.2% to 31.6%, 37.5% to 28.3%, and 35.7% to 22.7%

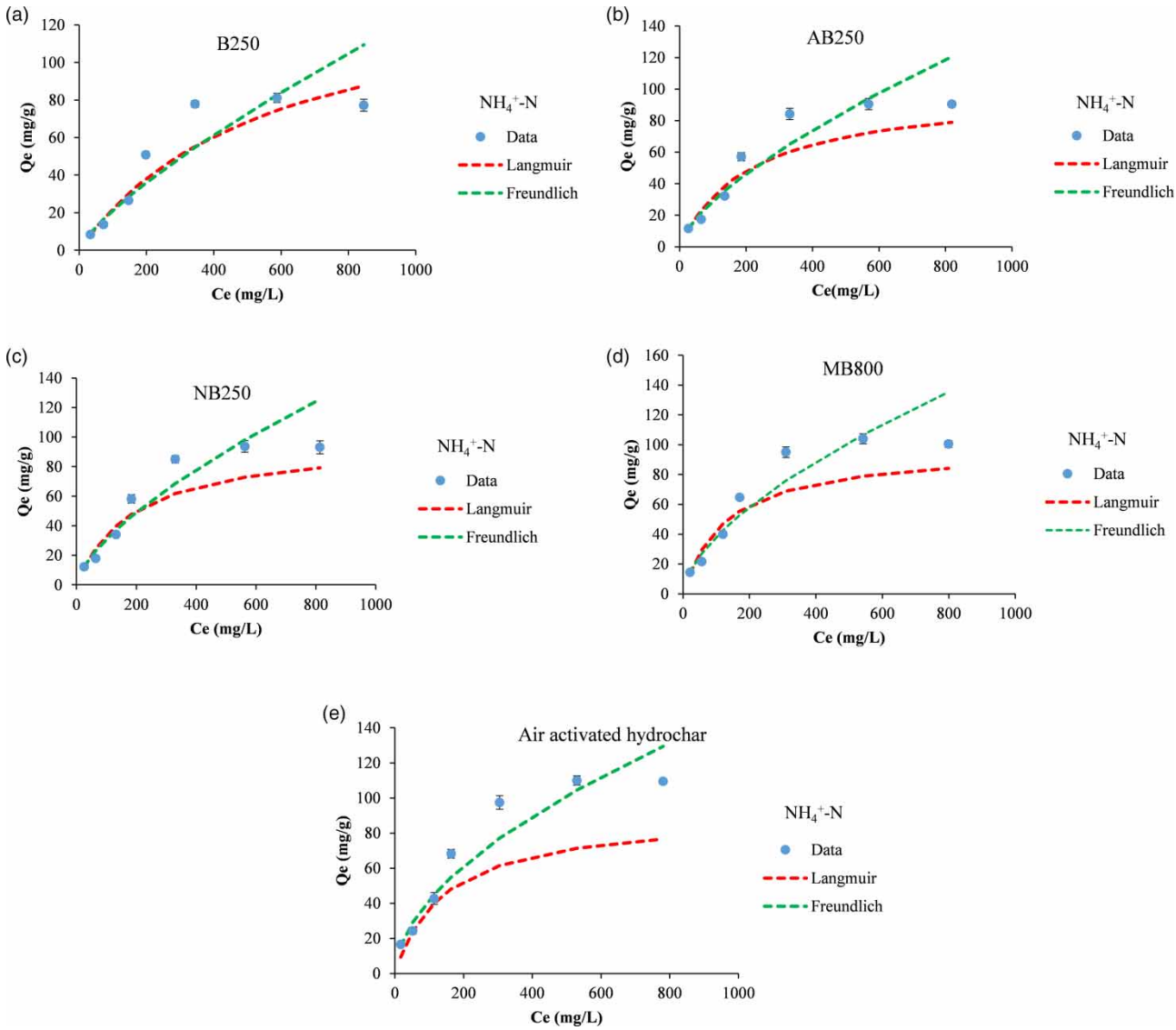


**Figure 4** | Adsorption isotherm of $NH_4^+$-N for 5 different hydrochar (a) B250, (b) AB250, (c) NB250, (d) MB800, and (e) air activated hydrochar.

for the use of water, acetic acid, and sodium hydroxide, respectively. The characterization showed that acetic acid or sodium hydroxide assisted HTC and activation with magnesium chloride or air could improve the surface properties. Acetic acid modification generated extensive oxygenated functional groups, while sodium hydroxide modification produced hydrochar with a high ratio of N/C and surface aromaticity. Treating hydrochar with magnesium chloride could impregnate nano-magnesium particles on the hydrochar, thereby improving the ability to remove N and P. Air activation of hydrochar resulted in a higher oxygen content.

The $NH_4^+$-N and $PO_4^{3-}$-P adsorption capacities of these hydrochars ranged from 92.6 to 122.4 mg/g and 1.6 to 15.8 mg/g, respectively. The adsorption capacity of hydrochars in swine wastewater is similar to the results of artificial wastewater. Despite the introduction of different surface functional groups, the hydrochars obtained by HTC assisted by acetic acid and sodium hydroxide did not significantly change the adsorption capacity of hydrochar. Hydrochar activated by using $MgCl_2$ and air substantially increased the adsorption capacity. The results suggested that Mg-nanoparticle dispersion and oxygen containing functional groups played a major role in adsorption than ion exchange and physisorption. Both $NH_4^+$-N and $PO_4^{3-}$-P adsorption fit the Freundlich model well.

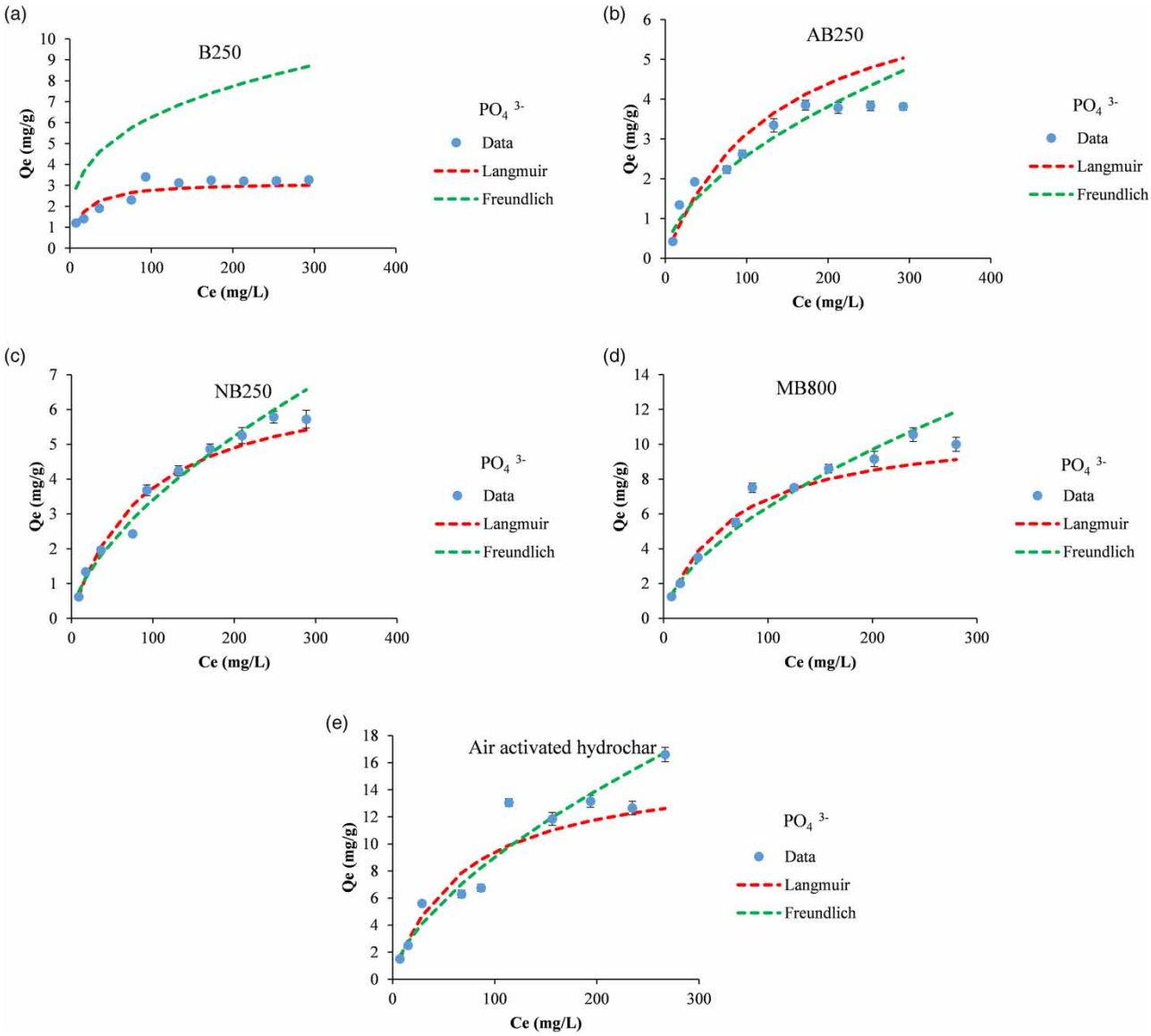


**Figure 5** | Adsorption isotherm of $PO_4^{3-}$ for five hydrochars. (a) B250, (b) AB250, (c) NB250, (d) MB800, and (e) air-activated hydrochar.

**Table 5** | Adsorption thermodynamics constants of $NH_4^+$-N and $PO_4^{3-}$-P of hydrochars

| | $NH_4^+$-N (Langmuir) | | | $NH_4^+$-N (Freundlich) | | | $PO_4^{3-}$-P (Langmuir) | | | $PO_4^{3-}$-P (Freundlich) | | |
|---|---|---|---|---|---|---|---|---|---|---|---|---|
| **Sample** | **$S_{max}$ (mg/g)** | **$K_L$ (L/mg)** | **$R^2$** | **$K_F$ (mg/g)** | **n** | **$R^2$** | **$S_{max}$ (mg/g)** | **$K_L$ (L/mg)** | **$R^2$** | **$K_F$ (mg/g)** | **n** | **$R^2$** |
| B250 | 147.08 | 0.0017 | 0.94 | 0.6096 | 1.29 | 0.95 | 3.16 | 0.07 | 0.87 | 1.54 | 3.29 | 0.91 |
| AB250 | 100 | 0.0045 | 0.93 | 1.2584 | 1.47 | 0.94 | 7.35 | 0.0074 | 0.89 | 0.19 | 1.79 | 0.92 |
| NB250 | 98.04 | 0.0051 | 0.93 | 1.4083 | 1.49 | 0.94 | 7.077 | 0.0112 | 0.97 | 0.20 | 1.61 | 0.98 |
| MB800 | 98.04 | 0.0076 | 0.92 | 2.2956 | 1.63 | 0.94 | 11.148 | 0.016 | 0.97 | 0.41 | 1.67 | 0.98 |
| Air-activated hydrochar | 90.90 | 0.91 | 0.98 | 3.3201 | 1.81 | 0.95 | 15.87 | 0.0145 | 0.97 | 0.49 | 1.58 | 0.98 |

## ACKNOWLEDGEMENTS

The publication was made possible by the United States Department of Agriculture (USDA NIFA award: NC.X-314-5-18-130-1) and the University of North Carolina's Research Opportunities Initiative (UNC ROI 2017-2020). This work was partially performed at the Joint School of Nanoscience and Nanoengineering, a member of Southeastern Nanotechnology Infrastructure Corridor (SENIC) and National Nanotechnology Coordinated Infrastructure (NNCI), which is supported by the National Science Foundation (ECCS-1542174).

## CONFLICT OF INTEREST

The authors declare that they have no conflict of interest.

## DATA AVAILABILITY STATEMENT

All relevant data are included in the paper or its Supplementary Information.

## REFERENCES

Banerjee, S., Chattopadhyaya, M. C., Srivastava, V. & Sharma, Y. C. 2014 Adsorption studies of methylene blue onto activated saw dust: kinetics, equilibrium, and thermodynamic studies. *Environmental Progress & Sustainable Energy* **33** (3), 790–799.

Bansal, S., Lishawa, S. C., Newman, S., Tangen, B. A., Wilcox, D., Albert, D., Anteau, M. J., Chimney, M. J., Cressey, R. L., DeKeyser, E., Elgersma, K. J., Finkelstein, S. A., Freeland, J., Grosshans, R., Klug, P. E., Larkin, D. J., Lawrence, B. A., Linz, G., Marburger, J., Noe, G., Otto, C., Reo, N., Richards, J., Richardson, C., Rodgers, L., Schrank, A. J., Svedarsky, D., Travis, S., Tuchman, N. & Windham-Myers, L. 2019 Typha (Cattail) invasion in north American wetlands: biology, regional problems, impacts, ecosystem services, and management. *Wetlands* **39** (4), 645–684.

Bekoe, D., Wang, L., Zhang, B., Todd, M. S. & Shahbazi, A. 2018 Aerobic treatment of swine manure to enhance anaerobic digestion and microalgal cultivation. *Journal of Environmental Science and Health, Part B* **53** (2), 145–151.

Bolisetty, S., Peydayesh, M. & Mezzenga, R. 2019 Sustainable technologies for water purification from heavy metals: review and analysis. *Chemical Society Reviews* **48** (2), 463–487.

Chen, J., Wang, L., Zhang, B., Li, R. & Shahbazi, A. 2018 Hydrothermal liquefaction enhanced by various chemicals as a means of sustainable dairy manure treatment. *Sustainability* **10** (1), 230.

Chintala, R., Schumacher, T. E., McDonald, L. M., Clay, D. E., Malo, D. D., Papiernik, S. K., Clay, S. A. & Julson, J. L. 2014 Phosphorus sorption and availability from biochars and soil/biochar mixtures. *CLEAN – Soil, Air, Water* **42** (5), 626–634.

Dubbe, D. R., Garver, E. G. & Pratt, D. C. 1988 Production of cattail (Typha spp.) biomass in Minnesota, USA. *Biomass* **17** (2), 79–104.

Fang, C., Zhang, T., Li, P., Jiang, R.-f. & Wang, Y.-c. 2014 Application of magnesium modified corn biochar for phosphorus removal and recovery from swine wastewater. *International Journal of Environmental Research and Public Health* **11** (9), 9217–9237.

Goel, P. 2006 *Water Pollution: Causes, Effects and Control*. New Age International Publishers, New Delhi, India.

Jaruwat, D., Udomsap, P., Chollacoop, N., Fuji, M. & Eiad-ua, A. 2018 Effects of hydrothermal temperature and time of hydrochar from Cattail leaves. In: *AIP Conference Proceedings*. AIP Publishing LLC, p. 020016.

Jiang, Y.-H., Li, A.-Y., Deng, H., Ye, C.-H., Wu, Y.-Q., Linmu, Y.-D. & Hang, H.-L. 2019 Characteristics of nitrogen and phosphorus adsorption by Mg-loaded biochar from different feedstocks. *Bioresource Technology* **276**, 183–189.

Jung, K.-W., Hwang, M.-J., Ahn, K.-H. & Ok, Y.-S. 2015 Kinetic study on phosphate removal from aqueous solution by biochar derived from peanut shell as renewable adsorptive media. *International Journal of Environmental Science and Technology* **12** (10), 3363–3372.

Kameyama, K., Miyamoto, T., Shiono, T. & Shinogi, Y. 2012 Influence of sugarcane bagasse-derived biochar application on nitrate leaching in Calcaric Dark Red Soil. *Journal of Environmental Quality* **41** (4), 1131–1137.

Khan, M. N. & Mohammad, F. 2014 Eutrophication: challenges and solutions. In: (Ansari, A. & Gill, S. (eds)) *Eutrophication: Causes, Consequences and Control*. Springer, Dordrecht, the Netherlands, pp. 1–15.

Kizito, S., Wu, S., Kirui, W. K., Lei, M., Lu, Q., Bah, H. & Dong, R. 2015 Evaluation of slow pyrolyzed wood and rice husks biochar for adsorption of ammonium nitrogen from piggery manure anaerobic digestate slurry. *Science of The Total Environment* **505**, 102–112.

Kostecke, R. M. 2002 *Effects of Cattail Management on Invertebrate Production and Migratory Bird use of Cheyenne Bottoms, KS.* PhD thesis, Texas Tech University, Lubbock, TX.

Mao, J., Zhang, K. & Chen, B. 2019 Linking hydrophobicity of biochar to the water repellency and water holding capacity of biochar-amended soil. *Environmental Pollution* **253**, 779–789.

Maurer, D. L., Koziel, J. A., Kalus, K., Andersen, D. S. & Opalinski, S. 2017 Pilot-scale testing of non-activated biochar for swine manure treatment and mitigation of ammonia, hydrogen sulfide, odorous volatile organic compounds (VOCs), and greenhouse gas emissions. *Sustainability* **9** (6), 929.

Oginni, O., Yakaboylu, G. A., Singh, K., Sabolsky, E. M., Unal-Tosun, G., Jaisi, D., Khanal, S. & Shah, A. 2020 Phosphorus adsorption behaviors of MgO modified biochars derived from waste woody biomass resources. *Journal of Environmental Chemical Engineering* **8** (2), 103723.

Reza, M. T., Rottler, E., Herklotz, L. & Wirth, B. 2015 Hydrothermal carbonization (HTC) of wheat straw: influence of feedwater pH prepared by acetic acid and potassium hydroxide. *Bioresource Technology* **182**, 336–344.

Sajjadi, B., Chen, W.-Y. & Egiebor, N. O. 2019 A comprehensive review on physical activation of biochar for energy and environmental applications. *Reviews in Chemical Engineering* **35** (6), 735–776.

Takaya, C., Fletcher, L., Singh, S., Anyikude, K. & Ross, A. 2016 Phosphate and ammonium sorption capacity of biochar and hydrochar from different wastes. *Chemosphere* **145**, 518–527.

Volpe, M., Goldfarb, J. L. & Fiori, L. 2018 Hydrothermal carbonization of *Opuntia ficus-indica* cladodes: role of process parameters on hydrochar properties. *Bioresource Technology* **247**, 310–318.

Wang, T., Zhai, Y., Zhu, Y., Peng, C., Xu, B., Wang, T., Li, C. & Zeng, G. 2017 Acetic acid and sodium hydroxide-aided hydrothermal carbonization of woody biomass for enhanced pelletization and fuel properties. *Energy & Fuels* **31** (11), 12200–8.

Xiu, S., Shahbazi, A. & Li, R. 2017 Characterization, modification and application of biochar for energy storage and catalysis: a review. *Trends in Renewable Energy* **3** (1), 86–101.

Xue, Y., Hou, H. & Zhu, S. 2009 Characteristics and mechanisms of phosphate adsorption onto basic oxygen furnace slag. *Journal of Hazardous Materials* **162** (2), 973–980.

Yamashita, T. & Yamamoto-Ikemoto, R. 2014 Nitrogen and phosphorus removal from wastewater treatment plant effluent via bacterial sulfate reduction in an anoxic bioreactor packed with wood and iron. *International Journal of Environmental Research and Public Health* **11** (9), 9835–9853.

Zeng, Z., Zhang, S.-d., Li, T.-q., Zhao, F.-l., He, Z.-l., Zhao, H.-p., Yang, X.-e., Wang, H.-l., Zhao, J. & Rafiq, M. T. 2013 Sorption of ammonium and phosphate from aqueous solution by biochar derived from phytoremediation plants. *Journal of Zhejiang University Science B* **14** (12), 1152–1161.

Zhang, B. & Wang, Y. 2013 *Biomass Processing, Conversion and Biorefinery*. Nova Science Publishers, Inc, New York, NY.

Zhang, B., Shahbaz, A., Wang, L., Whitmore, A. & Riddick, B. A. 2012 Fermentation of glucose and xylose in cattail processed by different pretreatment technologies. *BioResources* **7** (3), 2848–2859.

Zhang, B., Joseph, G., Wang, L., Li, X. & Shahbazi, A. 2020 Thermophilic anaerobic digestion of cattail and hydrothermal carbonization of the digestate for co-production of biomethane and hydrochar. *Journal of Environmental Science and Health, Part A* **55** (3), 230–238.

First received 7 May 2021; accepted in revised form 1 September 2021. Available online 14 September 2021